Antenna Study: Performance Enhancement

P. D. Potter
Communications Elements Research Section

A study of possible DSS 14 64-m-diameter antenna gain improvement by utilizing existing dual-reflector shaping techniques has been previously published. That study was restricted to the case of the axially symmetric (unicone) initial 64-m-diameter antenna configuration. After installation of the asymmetrical tricone system, studies of shaping techniques were discontinued pending operational experience with the tricone system at S- and X-bands, and development of new analytical tools for design and analysis of asymmetrical-shaped reflector systems. Recently, the required analytical tools have been developed and are described in this article.

I. Introduction

A study of possible DSS 14 64-m-diameter antenna gain improvement by utilizing existing dual-reflector shaping techniques has been previously published (Ref. 1). That study was restricted to the case of the axially symmetric (unicone) initial 64-m antenna configuration. After installation of the asymmetrical tricone system, studies of shaping techniques were discontinued pending operational experience with the tricone system at S- and X-bands, and development of new analytical tools for design and analysis of asymmetrical-shaped reflector systems. Recently, the required analytical tools have been developed and are described in this article.

Two techniques for obtaining enhanced performance of the DSS 14 64-m antenna have been investigated. Both provide frequency-independent improvement, and both are compatible with the tricone system. The first technique involves use of a shaped, asymmetric, nonhyperboloidal subreflector surface in conjunction with a readjustment of the main reflector panels to provide nearly uniform illumination of the antenna aperture and, hence, higher gain. As a part of such a system, the use of a 2-m surface extension (outriggers) has been investigated. The second technique involves covering the quadripod legs with metal plates to direct the scattered energy into the cold sky rather than the hot Earth. The noise temperature improvement afforded by this modification has been analyzed.

The two techniques mentioned above provide a gain improvement of approximately 0.8 to 1.4 dB (with and without outriggers, respectively) and a noise temperature improvement of 2 K, resulting in a figure of merit improvement of approximately 1.4 to 2.2 dB without outriggers and 2.0 to 3.4 dB with outriggers, depending on whether the configuration is optimized for listen-only, 2-way ranging or 2-way radar. This improvement is essentially independent of frequency and elevation angle.

II. Analytical Technique for Design of Asymmetrical-Shaped Dual-Reflector Antenna Systems

The method used for analyzing the shaped reflector modification is as follows: First, a shaped-reflector system is derived assuming a particular feedhorn and an axially symmetric geometry. The resulting main reflector surface is then used together with the tricone geometry to derive a nonsymmetric subreflector surface which preserves constant path length from the feedhorn to all points in the antenna aperture plane. The result is thus a frequency-independent design. Scattering patterns of this nonsymmetric feedhorn/subreflector combination are calculated, and the results are integrated to obtain aperture efficiency and spillover.

The basic approach for synthesizing the subreflector surface and its validity is based on a series of premises:

(1) In order to be compatible with the tricone configuration, the main reflector should be a figure of revolution.

(2) The nearly uniform aperture illumination which is achieved in a symmetrical, shaped system is a result of the ray distribution between the main reflector and the subreflector for a given subreflector illumination.

(3) The subreflector amplitude illumination for the off-axis tricone system is very nearly the same as for the symmetrical system.

(4) From (2) and (3), if the symmetrical, shaped main reflector design is utilized and a nonsymmetrical subreflector surface can be found which satisfies Snell's Law at each point of its surface, an exact frequency-independent phase solution will have been found and nearly uniform aperture illumination will result.

(5) There exists a continuous family of subreflector surfaces which satisfy Snell's Law at each point (this is assured by the principle of normal congruence) (Ref. 2, p. 125), and from the Law of Optical Path (Ref. 2, p. 125), all of these surfaces will result in a constant path length between the off-axis feed and the main reflector aperture plane. For each of these surfaces, however, the constant path length will be different.

(6) If a subreflector surface is computed, which results in constant path length from the feedhorn to the aperture plane, Snell's Law will be automatically satisfied for each point on the subreflector surface and the problem is solved. This premise is not immediately obvious, but may be demonstrated as follows [it is also implied, but not explicitly stated, by Silver (Ref. 2, pp. 127–128)].

Consider Fig. 1, with the main reflector surface S_1 given by the symmetrical shaping technique. The feedhorn is located at the point A. The plane of the figure contains the point A and ray 1, the latter's geometry being uniquely determined by the given surface S_1. S_2 is a hypothetical subreflector surface which obeys Snell's Law everywhere and passes through the point P. Consider another ray, ray 2, which intersects S_2 at the point P'. From the Law of Optical Path, the total length $APOQ$ equals the length $AP'O'Q'$. Still considering ray 2, consider some other intersection, point P''. It is clear from the geometry that any selection of P'' other than at P' will result in a different total path length. Thus, with the geometry of the main to subreflector rays given, a constraint of constant total path length is sufficient to ensure that the resulting subreflector surface obeys Snell's Law.

The first step is to calculate the phase and amplitude of the scattered subreflector patterns for the asymmetrical system and demonstrate that these are substantially the same as for the shaped symmetrical system. Consider the coordinate systems shown in Fig. 2. The feed is centered at the point O, with the Z-axis its longitudinal axis, which is taken to be in the plane determined by the main reflector (Z'') axis and the point O. By a straightforward coordinate transformation,

$$X'' = \rho(\cos\phi_R \sin\theta\cos\phi - \sin\phi_R\cos\theta) + R_D \equiv A_4\rho + R_D \quad (1)$$

$$Y'' = \rho\sin\theta\sin\phi = A_5\rho \quad (2)$$

$$Z'' = \rho(\sin\phi_R\sin\theta\cos\phi + \cos\phi_R\cos\theta) \equiv A_6\rho \quad (3)$$

where ρ, θ, ϕ are the polar coordinates of a point on the subreflector in the feed (X, Y, Z) coordinate system.

The next step is to determine the ρ values as a function of θ and ϕ such that intersections occur with rays from the main reflector as given by the symmetrical shaping program. Consider Fig. 3. The point O' is the origin of the X'', Y'', Z'' coordinate system. From geometry,

$$\tan\beta = \frac{H}{G} = \frac{X_p - [(X'')^2 + (Y'')^2]^{1/2}}{Y_p - A + Z''} \quad (4)$$

or

$$(X'')^2 + (Y'')^2 + A_1(Z'')^2 + A_2 Z'' + A_3 = 0 \quad (5)$$

where

$$A_1 \equiv -\tan^2\beta \tag{6}$$

$$A_2 \equiv 2\tan\beta\,[X_p - \tan\beta\,(Y_p - A)] \tag{7}$$

$$A_3 \equiv -[X_p^2 - 2X_p\tan\beta\,(Y_p - A) + \tan^2\beta\,(Y_p - A)^2] \tag{8}$$

Combining Eqs. (5) through (8) with Eqs. (1) through (3),

$$A_7\rho^2 + A_8\rho + A_9 = 0 \tag{9}$$

where

$$A_7 = A_4^2 + A_5^2 + A_1A_6^2 \tag{10}$$

$$A_8 = 2A_4R_D + A_2A_6 \tag{11}$$

$$A_9 = A_3 + R_D^2 \tag{12}$$

Thus, for each θ, ϕ direction, Eq. (9) may be solved to provide a table of ρ values corresponding to each point on the shaped main reflector surface. The next step is to determine, from this table, the correct $\rho\,(\theta, \phi)$ which satisfies the constant path length constraint. From Fig. 3,

$$\ell_1 = \rho \tag{13}$$

$$\ell_2 = G/\cos\beta = \frac{(Y_p - A)}{\cos\beta} + \frac{A_6\rho}{\cos\beta} \tag{14}$$

$$\ell_3 = Y_p \tag{15}$$

The total path length C_T is given by

$$C_T = \ell_1 + \ell_2 + \ell_3 = A_{10} + \left(1 + \frac{A_6}{\cos\beta}\right)\rho \tag{16}$$

where

$$A_{10} = [Y_p + (Y_p - A)/\cos\beta] \tag{17}$$

A set of C_T values, $C_T\,(N)$, is thus computed corresponding to each point on the main reflector surface. By search of this table, a pair of values is found which bracket the correct given value C_0. The correct ρ value is then found by interpolation between the corresponding pair of ρ values.

A computer program has been written and utilized to generate the subreflector coordinates and calculate the resulting scattered fields. Numerical results, which show excellent performance, will be given in a future reporting.

III. Noise Temperature Reduction by Quadripod Coverings

A number of tests have been performed in which the system noise temperature of a given feedcone has been measured both on the ground and when antenna-mounted. Although there is considerable scatter in the available data, the antenna-mounted temperatures are consistently higher by 2–4 K. This temperature increase arises primarily from four sources: (1) direct spillover of subreflector scattered energy past the paraboloid edge, (2) scattering of the subreflector scattered energy to the ground by the quadripod, (3) scattering of the feedhorn spillover by the quadripod to the ground, and (4) scattering of the antenna aperture radiation by the quadripod to the ground.

An attempt has been made to derive the observed antenna temperature increase by calculation. To perform this calculation, the antenna was taken to be pointed at zenith and the quadripod was assumed to scatter energy isotropically. A double integration of the scattered energy was performed; the first integration involved the amount of energy intercepted by the quadripod leg as a function of the position along the leg, and the second involved the solid angle subtended by the ground as a function of the position along the leg. Weighting by the amplitude illumination function was included. The results are in general agreement with the observed data and are given in Table 1.

In general, the components in Table 1 are difficult to experimentally verify. An attempt was made, however, to experimentally verify component number 5, the direct rear spillover. Since the edge of the antenna occurs at an angular position in the illumination function for which rapid cutoff occurs, this component should be a function of the subreflector axial position. The variation with axial position was calculated from subreflector scattered pattern data to be 0.0048 K per cm of subreflector travel. Data were taken[1] and showed a value of 0.0036 K per cm of travel. While this agreement is not perfect, it shows that the value for component 5 is not grossly in error.

Item 4 in the above table arises from the fact that some of the quadripod scattering is in low elevation angle directions. The value for this effect was obtained by integrating the sky temperature over all directions and subtracting out the zenith value.

It is proposed that items 2, 3, and 4 above may be virtually eliminated by covering the quadripod legs with metal sheets. Since the quadripod has been observed to

[1]By Dr. C. T. Stelzried, JPL Communications Elements Research Section.

behave as though it is essentially 100% opaque (by comparison of measured and calculated secondary patterns), such a modification should not significantly affect the antenna gain. The purpose of the leg coverings is to direct the quadripod scattering into the paraboloid and then into the cold sky. To evaluate this concept, a computer program was written to calculate the scattered energy ray directions. Because the quadripod is trapezoidal in cross section, there are four different ray paths to consider: (1) the ray from the antenna focus to the inner side of the quad leg to the paraboloid and out, (2) the ray from the antenna focus to the side of the quad leg to the paraboloid and out, (3) the ray from the aperture to the inner side of the quad leg and out, and (4) the ray from the aperture to the side of the quad leg and out. The calculations showed these ray directions to vary only slightly with position on the quad leg. The resulting ray directions are given in Table 2.

Thus, for evaluation angles above 10 deg, component 2 (Table 1) is eliminated. Component 3 is eliminated for elevation angles above 55 deg. Component 4 is eliminated and component 1 is reduced to 0.1 deg by use of the low subreflector edge illumination desired in the shaping procedure. Component 5 is a function of elevation angle below an elevation angle of 62 deg. Taking all of the components into account, Fig. 4 shows the differential antenna temperature as a function of elevation angle for the improved system. Also shown is the observed effect for the tricone/SCU configuration. This curve was obtained by subtracting the atmospheric noise contribution from the observed system temperature as a function of elevation angle. A constant noise component was then subtracted out to fit the differential antenna temperature to 3.0 K at zenith.

A final curve in Fig. 4 is the ratio of the existing to improved system noise temperatures versus elevation angle, expressed in dB improvement. It can be seen that the proposed technique of covering the quadripod legs offers an improvement of 0.5–0.6 dB as a function of elevation angle.

References

1. Ludwig, A. C., "Antennas for Space Communications: Shaped Reflector Cassegrainian Antennas," in *Supporting Research and Advanced Development,* Space Programs Summary 37-35, Vol. IV, pp. 266–268. Jet Propulsion Laboratory, Pasadena, Calif., Oct. 31, 1965.
2. Silver, S., *Microwave Antenna Theory and Design.* McGraw-Hill Book Co., Inc., New York, 1949.

Table 1. Calculated differential antenna temperature components

Component	Zenith noise contribution, K
1. Quadripod scattering of horn spillover	0.7
2. Quadripod scattering of subreflector illumination	0.8
3. Quadripod scattering of aperture radiation	0.7
4. Quadripod scattering to the atmosphere	0.1
5. Direct rear spillover	0.7
Total	3.0

Table 2. Quadripod ray directions to antenna axis

Ray	Direction, deg
1	10.2
2	0.1
3	54.8
4	4.9

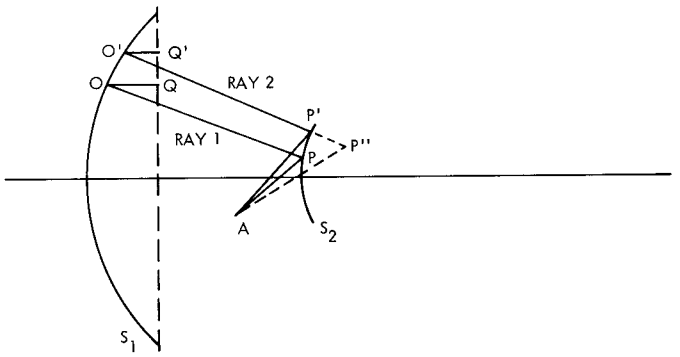

Fig. 1. Path length geometry

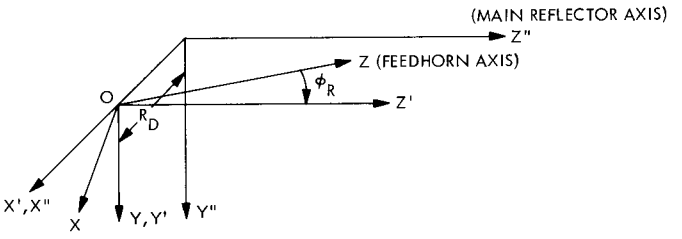

Fig. 2. Coordinate systems

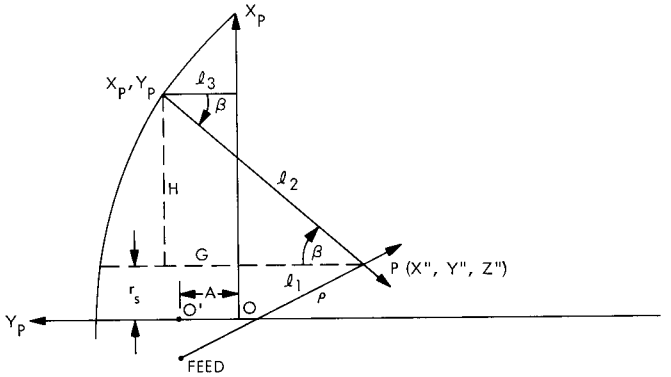

Fig. 3. Ray intersection geometry

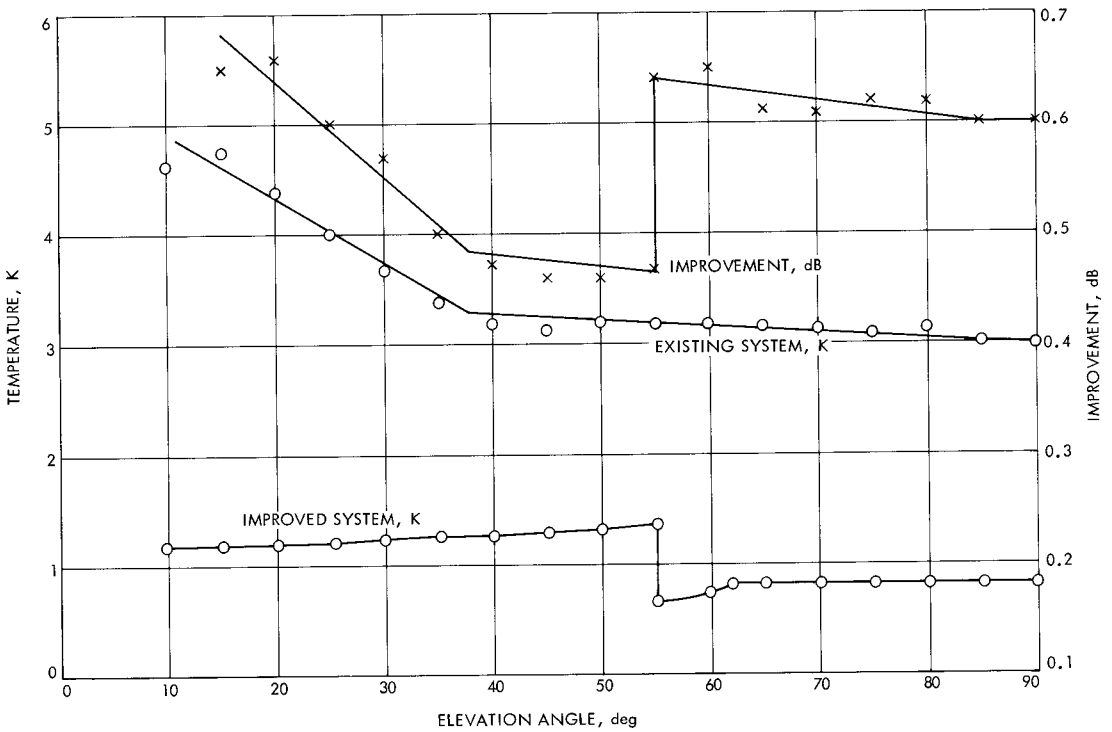

Fig. 4. Quadripod and spillover noise effect